Proceedings of MNHMT2009
Micro/Nanoscale Heat and Mass Transfer International Conference
December 18-21, 2009, Shanghai, China

MNHT2009-18276

Development of an Adaptive Vapor Chamber with Thermoresponsive Polymer Coating

Yuejun Zhao[#], Tao Chen[#], Xiaodong Zhang, Stefan Zauscher and Chuan-Hua Chen[*]
Department of Mechanical Engineering and Materials Science, Duke University, Durham, NC 27708

Abstract

We propose a novel concept for an adaptive vapor chamber using a thermoresponsive polymer coating to enhance heat transfer and reduce local thermal gradients. By coating the wick structures with stimulus-responsive polymer brushes with an upper critical solution temperature (UCST), the hotter surface becomes more wettable than the colder surface. The smaller contact angle at higher temperature generates larger capillary forces and promotes stronger return flow toward the hotspots. In this paper, we present our progress toward developing the adaptive vapor chamber. We have grafted poly(2-(meth-acryloyloxy)ethyl(dimethyl(3-sulfopropyl) ammonium hydroxide) (PMEDSAH) brushes on silica wafers, and the PMEDSAH polymer coating exhibits UCST properties with stable and tunable wettability. We have captured infrared images of the evaporator with steady and transient heating, and developed a thermographic technique that can be used to test the adaptive wick functionality in a vapor chamber.

Keywords: vapor chamber, adaptive wick, thermoresponsive polymer, infrared thermography

1. Introduction

Flat plate heat pipes, sometimes called vapor chambers, have very high thermal conductance and can be used for cooling high-power semiconductor chips and electronic equipments [1]. In a vapor chamber, heat is applied at the evaporator where the working fluid is vaporized, absorbing the latent heat of vaporization. The vapor then flows to the condenser where it condenses, releasing the latent heat of vaporization. A wick structure along the walls of the heat pipes/vapor chambers provides capillary forces to drive the liquid return from the condenser to the evaporator.

We propose a novel concept for an adaptive vapor chamber using a thermoresponsive polymer coating to improve heat transfer and reduce local thermal gradients. By coating the wick structure with a stimulus-responsive polymer of an upper critical solution temperature, the hotter surface becomes more wettable than the colder surface (Figure 1a). The capillary pressure across the liquid vapor interface, Δp_c, is given by

$$\Delta p_c = p_v - p_l = 2\sigma \cos\theta / r \quad (1)$$

where p_v is the vapor pressure, p_l is the liquid pressure, σ is the liquid surface tension, θ is the contact angle, and r is the radius of the (cylindrical) cavity (Figure 1b). While the surface tension decreases weakly with increasing temperature, the contact angle decreases strongly with temperature around the UCST. The net result is a significant increase in capillary pressure at hotspots (Eq. 1, Figure 1a), which promotes liquid return toward the hotspots. This adaptive process is expected to reduce the temperature gradients in the vapor chamber.

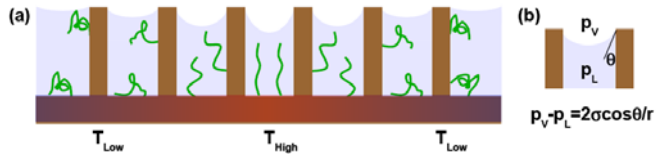

Figure 1. (a) Adaptive wick using a thermoresponsive polymer coating. (b) Capillary pressure across the liquid-vapor interface.

In this paper, we report our progress in the development of the adaptive wick, including the synthesis and characterization of UCST polymers, the fabrication of a prototype vapor chamber, and the development of an infrared imaging technique for testing the adaptive functionality.

2. UCST Polymer Synthesis

We have developed a surface-grafted polymer brush that exhibits reproducible UCST behavior, and shown that such thermoresponsive polymer is stable under repeated thermal cycling. Our findings suggest that this PMEDSAH polymer can potentially work as a coating for the adaptive wick.

2.1 Silane SAMs on Silicon Substrates

Silicon wafers were cleaned in a mixture of HO_2/H_2SO_4 in a water bath at 80°C for 30 min,washed thoroughly with Milli-Q-grade water, and dried in a stream of nitrogen. The clean silicon substrate was then immersed in an aqueous NaOH

solution (0.1 M) for 2 min and subsequently in HNO_3 (0.1 M) for 10 min to generate surface hydroxyl groups.

The ATRP initiator was (a) (11-(2-Bromo-2-methyl)propionyloxy)-undecyltrichlorosilane. Two non-initiators were used: (b) 3-aminopropyltrie thoxysilane; and (c) trichloro(octadecyl)silane. Their chemical structures are shown below:

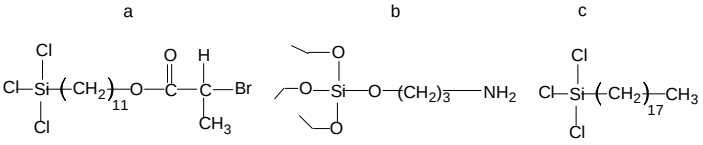

2.1.1 Initiator Silane on Silicon Substrates

A self-assembled monolayers (SAMs) of silane initiator was obtained by immersing clean Si substrates in a 1.0 vol% solution of the initiator (50 µL) in anhydrous toluene (5 mL) for 1 hr. After incubation, the substrates were washed with copious amounts of toluene, and rinsed in ethanol and DI water. The samples were subsequently dried in a stream of dry nitrogen and immediately transferred into the polymerization solution.

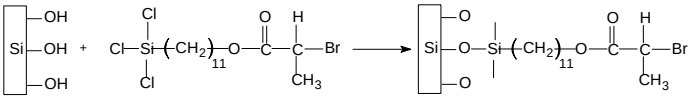

2.1.2 Mixed Silane Initiator and Non-initiator

A mixed SAM of silane initiator and non-initiator was obtained by immersing clean, Si substrates in a 1.0 vol% solution of the initiator (5 µL) plus non-initiator (45 µL) in anhydrous toluene (5 mL) for 1 hr. The initiator density was adjustable by changing the feed ratio of silane initiator and silane non-initiator.

2.2 Surface Grafted Polymer Brush

Poly (2-(meth-acryloyloxy)ethyl(dimethyl(3-sulfopropyl) ammonium hydroxide) (PMEDSAH) brushes were prepared in accordance with published protocols [2, 3] with some slight modifications based on our previous experience [3, 4]. Briefly, the polymerization solution was prepared by adding a solution of MEDSAH to an organometallic catalyst. The organometallic catalyst was formed in a N_2 atmosphere by adding CuBr and PMDETA in a 1:5 molar ratio to MeOH. The mixture was then sonicated for 1-2 min to form the CuBr/PMDETA complex. Next, MEDSAH in DI water was injected into the catalyst-complex using a syringe under oxygen exclusion. The polymerization solution was then transferred into flasks containing the sample substrates with immobilized initiator. The flasks were sealed with rubber septa under nitrogen. To obtain different brush heights, polymerization times were varied. After the desired reaction time, substrates were removed from the polymerization solution, exhaustively rinsed with DI water to remove all traces of the polymerization solution, and dried in a stream of nitrogen.

2.3 Wettability Control by Chemical Background

To control the wettability of the polymer brushes we synthesized PMEDSAH brushes on silica wafers using a mixture of a silane initiator and silane non-initiator. The contact angle change depends on the wettability of the substrate background, i.e., the area that is not covered with polymer brushes. This is illustrated by the range of contact angle changes as low as 10° with a hydrophilic non-initiator (Figure 2a) and as high as 50° with a hydrophobic non-initiator (Figure 2b).

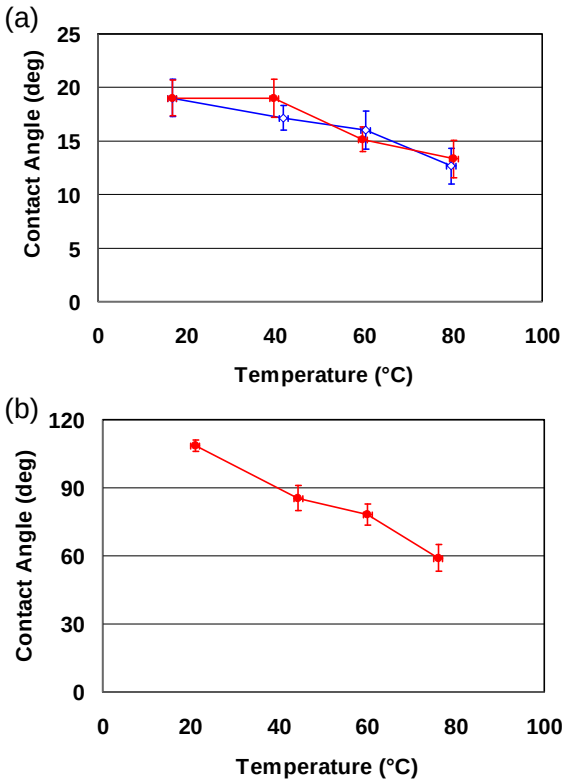

Figure 2. UCST behavior of PMEDSAH polymer can be tuned by non-initiator silane. The ATRP initiator is mixed with (a) a hydrophilic silane; and (b) a hydrophobic silane. The temperature was increased from 20 °C to 80 °C in both cases, and was reduced back to 20 °C in (a) to show reversibility.

The contact angle was measured using the captive bubble method, in which an air bubble was released to an inverted substrate, both immersed in a thermal bath. Compared to the sessile drop method, the captive bubble method better simulates the vapor chamber environment.

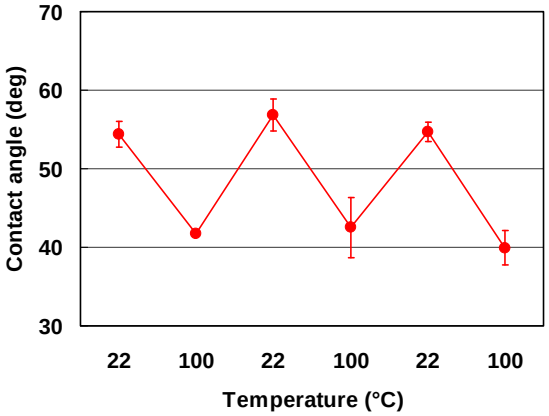

Figure 3. Reversible thermoresponsive behavior of PMEDSAH brushes (10% grafting density, brushes height ~75nm) after repeated thermal cycling between 22 °C and 100 °C.

2.4 Thermal Stability of Polymer Brushes

For PMEDSAH brushes synthesized from silane initiators, the thermoresponsive wettability is completely reversible and stable, as indicated by repeated thermal cycling between room temperature and 100 °C (Figure 3). Experiments performed after a few weeks yielded similar results, confirming the stability of the polymer coating and their thermoresponsive characteristics.

3. Vapor Chamber Fabrication

The adaptive wick needs to be tested in a vapor chamber. We have fabricated a vapor chamber as schematically shown in Figure 4. The evaporator was made of stainless steel (type 303, 16.3 W/m·K). The evaporator was 25 mm square and 1 mm thick with mechanically machined grooves as the wick structures. Each pillar in the wick structure was 0.4 mm square, 0.4 mm tall, and the squarely positioned pillars were 0.4 mm apart edge-to-edge. The condenser were made of pure copper (401 W/m·K) with the same wick structure as the evaporator. To promote capillarity-driven liquid return, parallel grooves were machines on the side walls of the vapor chamber, and each groove was 0.4 mm in width and 2 mm in depth. The vapor space was 2 mm in height.

Two copper tubes were attached to the vapor chamber, one as the vacuum port and the other as the charging port. The copper vacuum pipe was cut and sealed with a crimping tool (CHA Industries, KEL-375). The vapor chamber was evacuated with a vacuum pump (Edwards RV3), and mechanically sealed with O-rings.

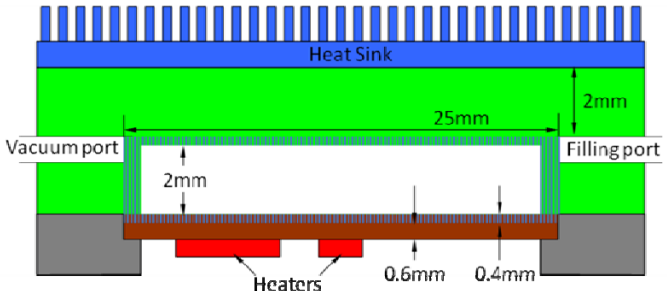

Figure 4. Schematic of a vapor chamber (not to scale).

Surface mounted resistors were used to simulate the sources of heat to be removed by the vapor chamber. The resistors were bonded to the stainless steel evaporator with an epoxy (Omega OB-200, 1.38 W/m·K). These 50 Ω-resistors were powered by a 0–36 V DC voltage source. An aluminum heat sink was attached to the condenser and cooled by an electric fan of the same size as the heat sink.

4. Thermographic Measurement

We developed an infrared imaging setup to be used in testing the adaptive wick and its effects on hotspot thermal management. The temperature distribution on the evaporator was monitored by an infrared imaging system (FLIR A325 with a 45° lens). To facilitate infrared thermography, a paint (Krylon® flat white) of known emissivity (0.99) was applied to the surface of the evaporator by multi-layer spray coating. The condenser temperature was measured by a thermocouple. Two surface mounted resistors were used to simulate steady and transient heat loads, respectively. The larger 6 mm×9 mm heater was supplied with a constant 10 V and was used to simulate steady-state heat load. The other 1 mm×3 mm heater was supplied with a pulsed voltage (10 V for a duration of 10 s). The separation between these two heaters was 2 mm.

The infrared images in Figure 5 were captured at the end of the 10 s-long voltage pulse. In Figure 5a, the vapor chamber was evacuated with no working fluid; In Figure 5b, the evacuated chamber was charged with 800 µL heptane. Note there was a small amount of heptane trapped between o-rings, and this volume should be excluded from the working fluid within the vapor chamber. The maximum surface temperature of the larger heater dropped from 100 °C for the evacuated case (Figure 5a) to 80 °C for the charged case (Figure 5b), while the base temperature was essentially the same (28.4 °C and 28.1 °C for Figures 5a and 5b, respectively). The transport of the working fluid driven by capillarity and phase change in the wick structure significantly enhanced heat transfer.

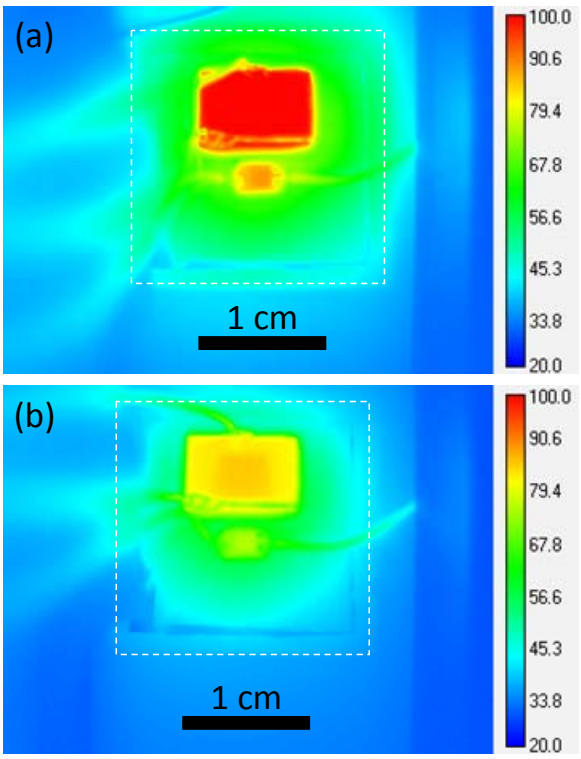

Figure 5. Infrared imaging of the evaporator of a vapor chamber with two surface-mounted heaters: (a) evacuated chamber; (b) charged chamber.

The hotspot effects on the temperature distribution were shown in Figure 6. Both images in Figure 6 represent the difference between the temperature map at the beginning and the end of the 10s pulsed heating. Compared to the evacuated case (Figure 6a), the charged vapor chamber (Figure 6b) was able to dissipate heat much more effectively, and therefore the hotspot effect was more localized and the maximum temperature rise was reduced in Figure 6b.

Although we have not tested the adaptive wick with thermoresponsive polymer coating, the thermographic results in Figure 6 suggest that infrared imaging may be used to test

the adaptive functionality in a vapor chamber, as the adaptive process will tend to reduce the temperature gradient.

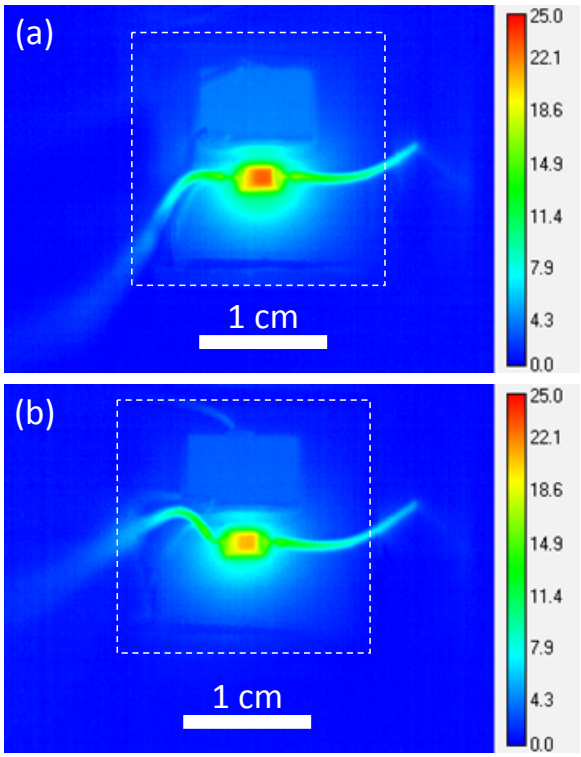

Figure 6. Temperature rise resulting from a transient hotspot on the evaporator: (a) evacuated chamber; (b) charged chamber.

5. Summary

In this paper we presented a novel concept for the adaptive vapor chamber using thermoresponsive polymer coating to enhance heat transfer and reduce local thermal gradients. At this point, we have developed protocols to synthesize a UCST polymer coating with tunable wettability and long-term thermal stability. We have also built a vapor chamber and developed a thermal imaging system to study hotspot effects on the vapor chamber. In future, we will build upon our progress in polymer synthesis and thermal testing to demonstrate the adaptive wick functionality.

6. Acknowledgements

This work was funded by DARPA under contract #N66001-08-C-2009 with T.W. Kenny as the program manager. The views, opinions, and/or findings contained in this article/presentation are those of the authors/presenters and should not be interpreted as representing the official views or policies, either expressed or implied, of the Defense Advanced Research Projects Agency or the Department of Defense. We appreciate helpful discussions with Q. Cai and C.L. Chen at Teledyne, and technical assistances from J.B. Boreyko and C.L. Lin at Duke.

References

[#] These authors contributed equally to the work.

[*] Email: chuanhua.chen@duke.edu

[1] D. A. Reay and P. A. Kew, *Heat Pipes: Theory, Design, and Applications*, 5th ed. Amsterdam: Butterworth-Heinemann, 2006.

[2] O. Azzaroni, *et al.*, "UCST wetting transitions of polyzwitterionic brushes driven by self-association," *Angew Chem Int Ed Engl*, vol. 45, pp. 1770-1774, 2006.

[3] N. Cheng, *et al.*, "Thickness-dependent properties of polyzwitterionic brushes," *Macromolecules*, vol. 41, pp. 6317-6321, 2008.

[4] M. Kaholek, *et al.*, "Stimulus-responsive poly(N-isopropylacrylamide) brushes and nanopatterns prepared by surface-initiated polymerization," *Chemistry of Materials*, vol. 16, pp. 3688-3696, 2004.

[5] M. Kaholek, *et al.*, "Fabrication of stimulus-responsive nanopatterned polymer brushes by scanning-probe lithography," *Nano Letters*, vol. 4, pp. 373-376, 2004.